# A Comparative Study on Crystal Structures and Synthetic Techniques of Ternary Hafnium/Zirconium Fluorides

**Navindra Keerthisinghe, Gyanendra B. Ayer, Mark D. Smith, and Hans-Conrad zur Loye***

*Department of Chemistry and Biochemistry, University of South Carolina, Columbia, SC, 29208, United States*

*Corresponding author. E-mail: zurloye@mailbox.sc.edu

## Abstract

Mild hydrothermal synthesis was employed to grow high-quality single crystals of ternary fluoridohafnates at low temperatures. The series of new materials was characterized using single crystal X-ray diffraction, and the crystal structures for $AHfF_6$ (A= Mg and Sr), $A_2HfF_8$ (A= Ba and Pb), $Ca_5Hf_3F_{22}$ and $Cd_2HfF_8(H_2O)_6$ are discussed herein. Although some material compositions have similar stoichiometries, all the compositions adopt different structural motifs. A comparison of the crystal structures and synthesis techniques of ternary fluoridohafnates and ternary fluoridozirconates is also reported, and the impact of the subtle changes of synthesis conditions on overall structures is discussed.

## Introduction

The chemistry of inorganic fluorides has been explored for many decades and, during this time, numerous synthetic routes were developed and used for the preparation of new inorganic fluorides, to determine their structures and to investigate their physical properties.[1] Often solid-state reactions were explored to prepare new compositions, utilizing mostly binary fluorides that were prepared by the direct fluorination of oxides or chlorides using $F_2$(g).[2–5] Solution routes, also, were explored, in particular those involving condensed anhydrous HF, resulting in the discovery and characterization of a very large number of phases.[6–8] An alternative approach utilized hydrothermal routes under supercritical conditions, which permits the formation of high-quality single crystals of novel compositions and structures.[9–12] Another solution route involved molten salts, which can be used at temperatures ranging from as low as ~150°C to over 1000 °C, depending on the particular salt chosen.[13–16] This approach also has been extremely fruitful and has yielded many new compositions and structures. More recently, the mild hydrothermal route has become popular as it can be used for the crystallization of fluorides and/or oxyfluorides, and also because it uses only small quantities of aqueous HF, which are easily handled in typical research laboratories.

In our group, we have used both molten salt synthesis[17–22] and mild hydrothermal synthesis[23–28] for the growth of single crystals of a large variety of fluoride phases. For the hydrothermal route using aqueous HF, we established that mild conditions, 160-200 °C and relatively short reaction times, 24 hrs, followed by slow cooling to room temperature, often yielded high quality crystals of ternary and quaternary fluorides whose structures could readily be

determined. We have used this approach to explore, in general, the preparation of transition metal and rare earth containing fluorides and oxyfluorides, including vanadates, niobates, tantalates, tungstates, molybdates, manganates, cobaltates, nickelates, cerates, as well as numerous actinide containing fluoride phases containing Th, U, Np, Pu, and Am.[7, 20, 23–26, 29–33] During this process, by experience, we have learned much about how to choose the optimum reaction conditions. In recent work we explored hafnium fluorides, which yielded a number of hydrated phases, including $Cs_2[M(H_2O)_6][Hf_2F_{12}]$ (M= Ni, Co, and Zn), and $CuHfF_6(H_2O)_4$.[34] To determine if we could adjust the reaction conditions to crystallize anhydrous hafnium fluoride phases, we further explored the mild hydrothermal reaction method. Herein we describe the synthesis and structural characterization of a series of anhydrous ternary hafnium fluorides, as well as of a new hydrated hafnium fluoride composition, that we obtained. In addition, we review the synthesis conditions and crystal structures of previously reported fluoridozirconates and fluoridohafnates to illustrate and to provide better insights into the ternary hafnium/zirconium fluoride phase space.

## Experimental

*Synthesis*

$HfO_2$ (Alfa Aesar, 99.9%), $Mg(CH_3COO)_2•4H_2O$ (Aldrich, 99.9%), $Ca(CH_3COO)_2•xH_2O$ (Alfa Aesar, 99%), $Sr(CH_3COO)_2$ (Alfa Aesar, 98%), $Ba(CH_3COO)_2$ (Alfa Aesar, 99%), $CdF_2$ (Acros Organics, 99.9 %), $Pb(CH_3COO)_2•3H_2O$ (Acros Organics, 99.9 %), $HNO_3$ (Sigma Aldrich, 37%), and HF (EMD, 49%) were used as received.

*Warning! HF should only be handled in a well-ventilated space, and proper safety precautions must be used. Proper treatment procedures should be followed immediately if contact with the liquid or vapor occurs.*

Single crystals of the reported compounds were grown via a mild hydrothermal route using $HfO_2$ and the respective divalent metal acetates or fluorides as the starting materials. For the preparation of $MgHfF_6$, $Ca_5Hf_3F_{22}$, *o*-$SrHfF_6$, *t*-$SrHfF_6$, $Ba_2HfF_8$, $Pb_2HfF_8$ and $Cd_2HfF_8(H_2O)_6$, 1 mmol of $HfO_2$, 0.25 ml of 37% $HNO_3$, and 1.00 ml of 49% HF were combined with 1 mmol of $Mg(CH_3COO)_2•4H_2O$, $Ca(CH_3COO)_2•xH_2O$, $Sr(CH_3COO)_2$, $Ba(CH_3COO)_2$,

$Pb(CH_3COO)_2 \cdot 3H_2O$, and $CdF_2$, respectively. The respective solutions were loaded into 23 ml PTFE-lined autoclaves. The autoclaves were sealed, heated to 160°C at a rate of 5 °C $min^{-1}$, held at this temperature for 24 hours, and then cooled to room temperature at a rate of 6 °C $h^{-1}$. The resulting single-crystal products were isolated from the solution by filtration and washed with water and acetone. The reaction yielded colorless crystals for Mg, Ca, Sr, Ba, Pb, and Cd containing compounds in a nearly quantitative yield based on $HfO_2$. Despite numerous attempts to obtain iron-containing hafnium fluorides, the main reaction product was always $FeF_3$.

*Single-Crystal X-ray Diffraction (SXRD)*

Single-crystal X-ray diffraction data were collected at ambient temperature using a Bruker D8 QUEST diffractometer equipped with a PHOTON-II area detector and an Incoatec microfocus source (Mo Kα radiation, λ = 0.71073 Å). The crystals were epoxied onto plastic supports. The raw area detector data frames were reduced and corrected for absorption effects using the SAINT+ and SADABS programs.[35, 36] Initial structural models were obtained with SHELXT using the dual-space technique.[37, 38] Subsequent difference Fourier calculations and full-matrix least-squares refinement against $F^2$ were performed with SHELXL-2018 using ShelXle.[39] Single crystal data is given in Table 1.

*Powder X-ray Diffraction (PXRD)*

Powder X-ray diffraction data for phase identification were collected on polycrystalline samples consisting of ground single crystals (Figures S2–S7). Data were collected on a Bruker D2 PHASER diffractometer using Cu Kα radiation over a $2\theta$ range of 5–65° with a step size of 0.02°.

Table 1. Crystallographic data for **1-7**

| Material | **$MgHfF_6$ (1)** | **$Ca_5Hf_3F_{22}$ (2)** | **$Ba_2HfF_8$ (3)** | **$Pb_2HfF_8$ (4)** | ***o*-$SrHfF_6$ (5)** | ***t*-$SrHfF_6$ (6)** | **$Cd_2HfF_8(H_2O)_6$ (7)** |
|---|---|---|---|---|---|---|---|
| Formula weight | 316.77 | 1154.24 | 605.17 | 744.87 | 380.11 | 380.11 | 663.39 |
| Crystal system | cubic | orthorhombic | orthorhombic | orthorhombic | orthorhombic | triclinic | monoclinic |
| Space group, Z | *Fm*–3*m,* 4 | $P2_12_12$, 2 | *Pnma*, 4 | $Pna2_1$, 4 | *Cmme*, 4 | *P*–1*,* 4 | *C*2/*c,* 4 |
| a, Å | 7.91630(6) | 9.9515(5) | 9.7329(3) | 10.0521(2) | 7.5160(3) | 7.0129(2) | 11.4354(3) |
| b, Å | | 7.3884(3) | 5.60874(19) | 11.6322(3) | 10.8895(5) | 8.1803(3) | 8.1989(2) |
| c, Å | | 9.9054(5) | 11.8810(4) | 5.32649(12) | 5.3224(2) | 8.3085(2) | 12.7713(3) |
| α, deg | | | | | | 102.2141(9) | |
| β, deg | | | | | | 96.3670(9) | 111.2510(10) |
| γ, deg | | | | | | 115.1462(8) | |
| V, $Å^3$ | 496.097(11) | 728.30(6) | 648.58(4) | 622.82(2) | 435.61(3) | 410.69(2) | 1115.99(5) |
| $\rho_{calcd}$, $g/cm^3$ | 4.241 | 5.263 | 6.198 | 7.944 | 5.796 | 6.148 | 3.948 |
| Radiation (λ, Å) | $MoK_\alpha$ (0.71073) | | | | | | |
| μ, $mm^{-1}$ | 21.181 | 23.355 | 28.069 | 70.654 | 36.095 | 38.285 | 13.181 |
| F(000) | 552 | 1028 | 1024 | 1232 | 656 | 656 | 1200 |
| T, K | 301 (2) | | | | | | |
| Crystal dim.,$mm^3$ | 0.08×0.08×0.08 | 0.05×0.03×0.01 | 0.08×0.02×0.01 | 0.06×0.04×0.02 | 0.12×0.08×0.02 | 0.18×0.04×0.02 | 0.07×0.06×0.05 |
| 2$\theta$ range, deg. | 4.459 – 44.524 | 2.901 – 33.180 | 5.41 – 70.078 | 2.678 – 34.976 | 3.742 – 40.283 | 2.872 – 40.305 | 6.27 – 59.964 |
| Reflections collected | 5814 | 37839 | 3778 | 3355 | 9289 | 35266 | 24289 |
| Data/restraints/ parameters | 137/0/7 | 2793/0/141 | 3778/0/60 | 3355/1/106 | 747 /0/24 | 5177/0/149 | 1618/6/103 |
| $R_{int}$ | 0.0461 | 0.0473 | 0.0354 | 0.0643 | 0.0526 | 0.0379 | 0.0345 |
| Goodness of fit | 1.208 | 1.244 | 1.136 | 1.102 | 1.131 | 1.169 | 1.131 |
| $R_1(I > 2\sigma(I))$ | 0.0073 | 0.0199 | 0.0143 | 0.0239 | 0.0164 | 0.0180 | 0.0098 |
| $wR_2$ (all data) | 0.0171 | 0.0529 | 0.0346 | 0.0643 | 0.0377 | 0.0459 | 0.0211 |
| Largest diff. peak/hole, $e·Å^{-3}$ | 0.67/–0.76 | 2.29/–1.76 | 1.02/–1.23 | 2.40/–1.76 | 1.53/–1.02 | 2.58/–1.72 | 0.53/–0.84 |

## Results and Discussion

*Synthesis*

Mild hydrothermal synthesis was utilized to obtain a series of ternary hafnium fluorides consisting of high-quality single crystals suitable for single-crystal X-ray diffraction. The synthesis was carried out at a very low temperature of 160 °C, in contrast to the very high temperatures (>700 °C) used in typical solid state ternary hafnium-containing fluoride synthesis.[40–43] Here, the highly reactive hydrofluoric acid acts as a mineralizer as well as a fluorinating reagent and $HNO_3$ lowers the pH.[23, 34] These reaction conditions, optimized via an Edisonian approach, enable the fluorination of the stable $HfO_2$ and allow the formation of ternary fluoride crystals at such low temperatures. The use of different divalent cations, Mg, Ca, Sr, Ba, Pb, and Cd, likely for size reasons, did not result in an isotypic series but rather resulted in a variety of different crystal structures reported herein (Figure 1).

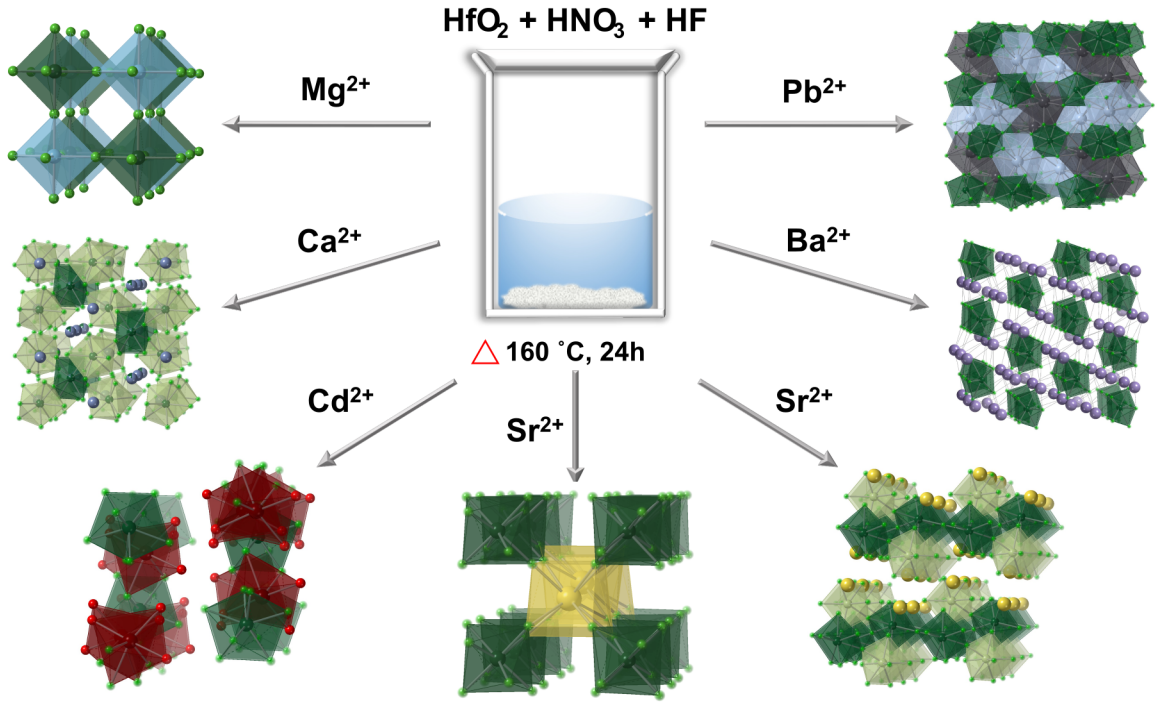


Figure 1. Schematic for the preparation of ternary hafnium-containing fluorides (**1-7**).

*Crystal Structure Descriptions*

$MgHfF_6$

Compound **1** crystallizes in the cubic space group *Fm*–3*m* and is isostructural with the previously reported zirconium analog, $MgZrF_6$.[44] The crystal structure of compound **1** was previously reported based on a Rietveld refinement of powder X-ray diffraction data by Bandemehr et al. in 2021.[5] Herein, we report a structure solution obtained using single crystal X-ray diffraction data. The structure is best described as a double $ReO_3$-type structure, where the $MgF_6$ and $HfF_6$ octahedra are ordered in a NaCl fashion. The $ReO_3$ structure can be thought of as a simple cubic perovskite structure ($ABX_3$) missing the A cation.[44] The three-dimensional framework of $MgHfF_6$ consists of corner-shared $MgF_6$ and $HfF_6$ octahedra. See Figure 2. The $MgF_6$ and $HfF_6$ coordination environments both have octahedral symmetry with Mg–F and Hf–F bond lengths of 1.971(15) Å and 1.987(15) Å, respectively.

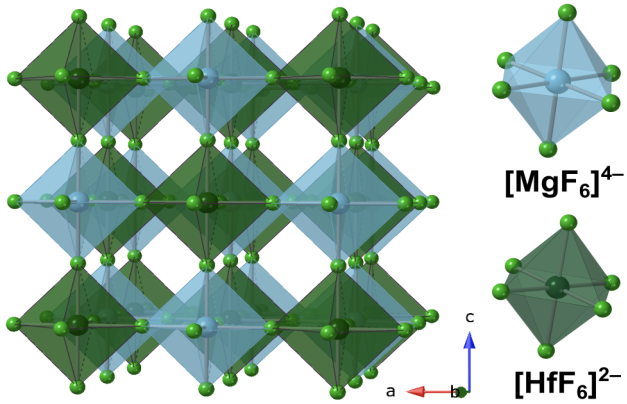


Figure 2. View of $MgHfF_6$ down the b-axis (left). Individual octahedra of $[MgF_6]^{4-}$ and $[HfF_6]^{2-}$ (right). Mg and Hf are shown as blue and dark green octahedra, respectively. F atoms are shown as green spheres.

$Ca_5Hf_3F_{22}$

Compound **2**, containing the larger (relative to magnesium) calcium cation, crystallizes in the orthorhombic crystal system in the non-centrosymmetric space group $P2_12_12$. The asymmetric unit consists of one hafnium site (Hf1), three calcium sites (Ca1-Ca3), two mixed hafnium/calcium sites (Hf2/Ca2A and Ca4/Hf4A), and eleven fluorine sites (F1-F11). The two mixed hafnium/calcium sites were modeled as having engaged in anti-site mixing, resulting in a refined occupancy of 85%Hf/15%Ca and 15%Hf/85%Ca, generating a perfectly electroneutral

composition without restraints. Both pure Hf(1) and mixed Hf(2) sites are coordinated to eight fluorine atoms to take on a distorted square-antiprismatic coordination environment. The two distinct $Hf(1)F_8$ (light green) and $Hf(2)F_8$ (dark green) polyhedra are located in trans-corner sharing chains, which in turn are cross-linked to yield a layered structure (Figure 3). The Ca(1) and mixed Ca(4) sites reside within the layers, while Ca(2) and Ca(3) are located in between the layers (Figure 3). The material is isotypic with its zirconium analogs of $Ca_5Zr_3F_{22}$[45] and $Sr_5Zr_3F_{22}$.[46]

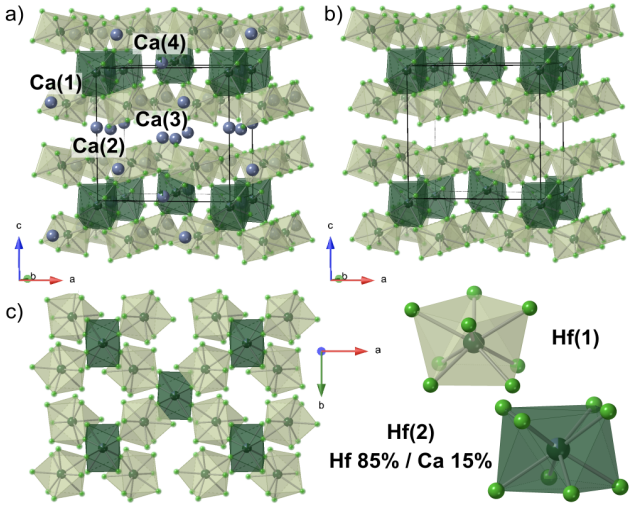


Figure 3. View of $Ca_5Hf_3F_{22}$ parallel to the *ac* plane (a). View of the layered structure framework (b). View of an extracted hafnium layer and the two individual hafnium sites (c).

$Ba_2HfF_8$

Compound **3**, incorporating the largest alkaline earth cation, Ba, crystallizes in the orthorhombic space group *Pnma*. The asymmetric unit consists of two unique barium sites, five fluorine sites, and a single hafnium site. It is isostructural with the zirconium analog $BaZrF_8$, previously reported by Le Bail and Laval.[42] The structure of $Ba_2HfF_8$ consists of isolated, distorted $[HfF_8]^{4-}$ square antiprisms separated from each other by the large $Ba^{2+}$ cations (Figure 4). The barium atoms are located in a $Ba(1)F_{12}$ cuboctahedra and a $Ba(2)F_{13}$ irregular polyhedra, as is also the case for $Ba_2ZrF_8$ (Figure 6). This material was previously studied for its optical properties by Hong Li et al. in 2020.[8]

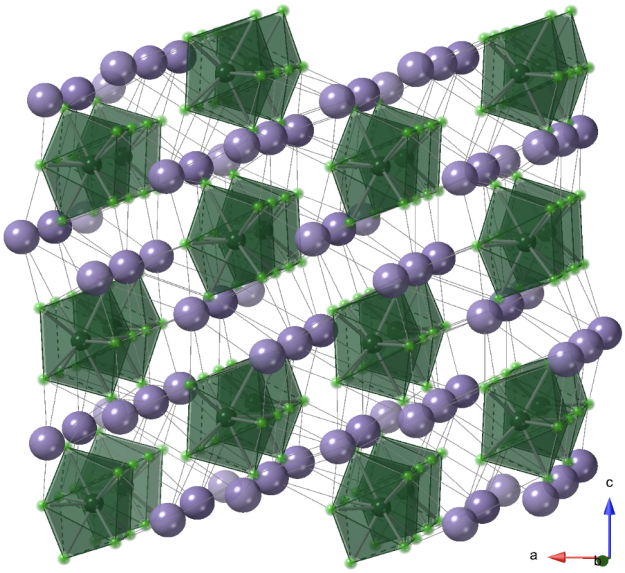


Figure 4. The crystal structure of $Ba_2HfF_8$ shown oriented parallel to the *ac* plane. Hf, Ba, and F are shown in dark green, purple, and green spheres respectively.

$Pb_2HfF_8$

Compound **4** crystallizes in the orthorhombic space group *Pna*$2_1$. The structure consists of two unique lead sites, eight fluorine sites, and a single hafnium site. The two 10 and 12 coordinated lead cations are located in $Pb(1)F_{10}$ and $Pb(2)F_{12}$ irregular polyhedra. These polyhedra connect to form two chains, one containing $Pb(1)F_{10}$ and one containing $Pb(2)F_{12}$ polyhedra. (Figure 5a) In both cases, the polyhedra within each chain are corner- and edge-sharing with each other. The chains run along the *c*-axis and connect to each other via edge- and face-sharing to create the 3-D lead-fluorine framework (Figure 5b and 5c) that contains cavities in which the hafnium cations are located as $HfF_8$ distorted square-antiprisms (Figure 5d). The zirconium analog of this material was synthesized by Laval et al. 1998. In that paper, the authors refer to $Pb_2ZrF_8$ as being isostructural to $Ba_2ZrF_8$. However, a comparison of the crystal structures indicates that $Pb_2ZrF_8$ crystallizes in orthorhombic space group *Pna*$2_1$, as does $Pb_2HfF_8$, while $Ba_2ZrF_8$ crystallizes in the space group *Pnma*.[42]

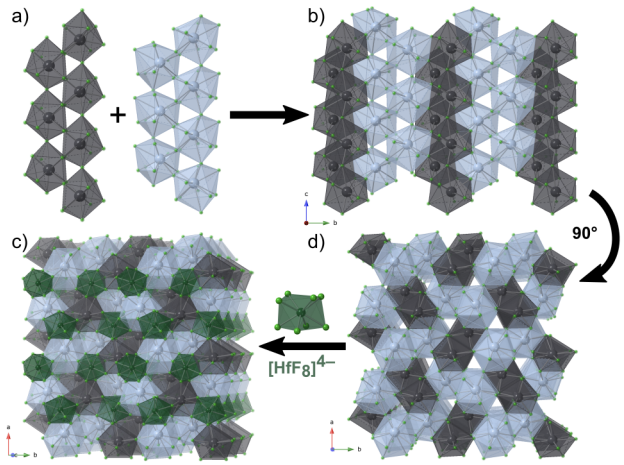


Figure 5. Chain 1 of $[Pb(1)F_{10}]^{8-}{}_n$ and chain 2 of $[Pb(2)F_{12}]^{10-}{}_n$ (a). View of a single layer of $[Pb_2F_{18}]^{14-}{}_n$ in the *bc* plane (b). View of $Pb_2HfF_8$ down the a-axis (c). View of the three-dimensional lead framework (d) parallel to the *ab* plane.

A comparison between compound **3** ($Ba_2HfF_8$) and compound **4** ($Pb_2HfF_8$) is warranted as they have the same overall stoichiometry. The change from Ba to Pb causes a change in the space group from orthorhombic *Pnma* to orthorhombic $Pna2_1$, presumably due to the slight differences in the coordination environments of Ba and Pb (Figure 6). These changes are presumed to be the result of the stereochemical influence of the $6s^2$ lone pair on Pb. These changes are also observed in the zirconium analogs, $Ba_2ZrF_8$ and $Pb_2ZrF_8$, and were reported by Le Bail and Laval in 1998.[42]

| | $Ba(1)F_{12}$ | $Ba(2)F_{13}$ | $HfF_8$ |
|---|---|---|---|
| $Ba_2HfF_8$ | 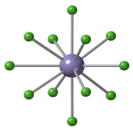 | 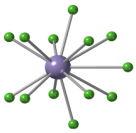 | 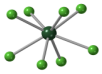 |
| M — F (Å) | 2.715 – 3.378 | 2.689 – 2.963 | 2.052 – 2.217 |
| | $Pb(1)F_{10}$ | $Pb(2)F_{12}$ | $HfF_8$ |
| $Pb_2HfF_8$ | 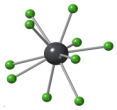 | 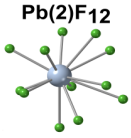 |  |
| M — F (Å) | 2.473 – 2.908 | 2.381 – 3.389 | 2.066 – 2.117 |

Figure 6. Comparison of the coordination environments of the metals in $Ba_2HfF_8$ and $Pb_2HfF_8$.

*o*-$SrHfF_6$ and *t*-$SrHfF_6$

The composition $SrHfF_6$ was previously reported,[41] albeit as a polymorph ($\alpha$-$SrHfF_6$) different from what we observe for *o*-$SrHfF_6$ and *t*-$SrHfF_6$, two new polymorphs that resulted from

our mild hydrothermal synthetic approach. By comparison, $\alpha$-$SrHfF_6$ was prepared by a solid-state reaction between anhydrous $SrF_2$ and $HfF_4$ at 973 K. $\alpha$-$SrHfF_6$ was found to crystallize in the monoclinic space group $P2_1/c$, while the two new polymorphs crystallize in the orthorhombic (*Cmme*) and triclinic ($P$–1) space groups, respectively.[41] Both crystals were isolated from the same reaction and were distinguishable from each other by their different crystal morphologies; the *o*-$SrHfF_6$ crystals had a rectangular shape, while the *t*-$SrHfF_6$ crystals were parallelogram shaped.

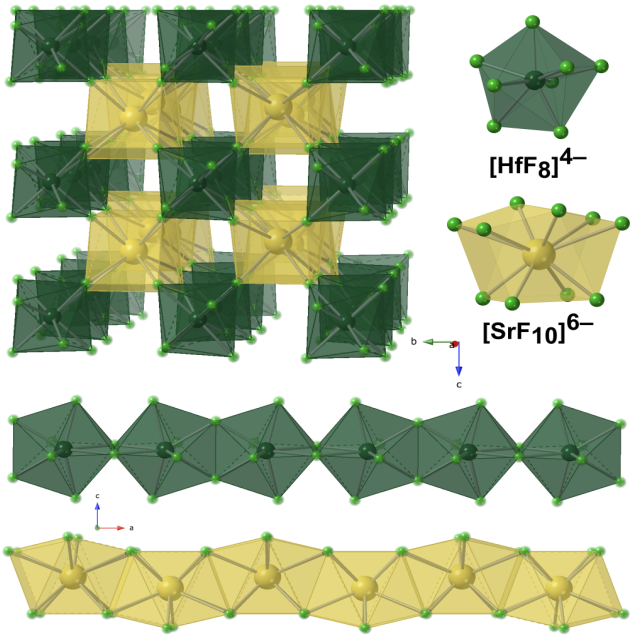


Figure 7. View on *o*-$SrHfF_6$ on the *bc* plane (top left). The $[HfF_8]^{4-}$ and $[SrF_{10}]^{8-}$ coordination polyhedra (top right). The trans-edge-sharing chain of $[Hf_2F_{14}]^{6-}{}_n$ and face-sharing chain of $[SrF_{10}]^{8-}{}_n$ (bottom).

In *o*-$SrHfF_6$, the asymmetric unit consists of two unique fluorine sites, a single strontium site, and a single hafnium site. Unlike in other structures mentioned herein, in this structure hafnium is in a snub disphenoid polyhedral coordination environment rather than in the usual distorted square antiprism (Figure 7).[41] The snub disphenoid polyhedral shape can best be described as a bicapped pentagonal pyramid with an additional two triangular faces. The Hf–F bond lengths are 2.0151(11) Å and 2.2077(8) Å for Hf–F(1) and Hf–F(2), respectively. The structure consists of trans-edge-shared chains of $[HfF_8]^{4-}$ polyhedra and chains of face-sharing $[SrF_{10}]^{8-}$ polyhedra. The two chains are corner-shared via F(1) atoms to build up the 3-D framework (Figure 7).

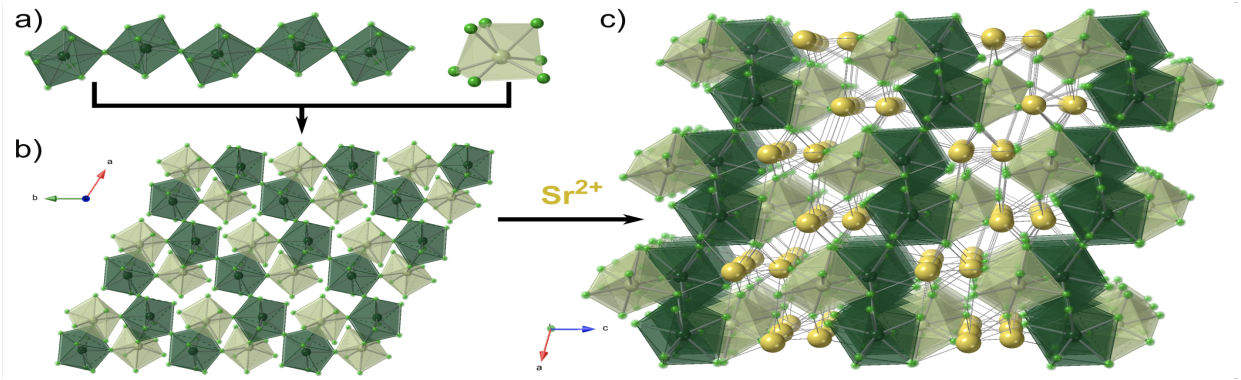


Figure 8. The zig-zag chains of $[Hf(2)F_8]^{4-}$ polyhedra and a single $[Hf(1)F_7]^{3-}$ pentagonal bipyramid (a). View of hafnium sheets in the *ab* plane (b). View of *t*-$SrHfF_6$ down the c axis. (c).

The asymmetric unit of *t*-$SrHfF_6$ consists of two unique hafnium sites, two strontium sites, and thirteen fluorine sites. Here, Hf(1) is coordinated to seven fluorine atoms and is in a pentagonal bipyramidal coordination environment, while Hf(2) is coordinated to eight fluorine atoms in a distorted square antiprismatic environment. The $[Hf(2)F_8]^{4-}$ polyhedra corner-share with each other to form a zig-zag chain that runs along the c-axis. These chains are linked to each other via corner-sharing $[Hf(1)F_7]^{3-}$ polyhedra to form four and eight-membered hafnium rings (Figure 8b and Figure 9). The strontium cations are located within the hafnium sheets and link the sheets to each other (Figure 8c).

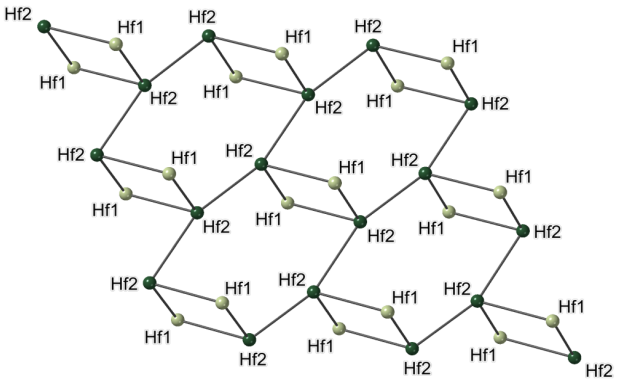


Figure 9. Hafnium cation network in *t*-$SrHfF_6$

$Cd_2HfF_8(H_2O)_6$

Compound **7** crystallizes in the monoclinic space group *C2/c*. The material consists of $[HfF_8]^{4-}$ distorted square antiprisms and $[CdF_3(H_2O)_3]^{-}$ distorted octahedra. The framework

structure is built up of trimers consisting of one $[HfF_8]^{4-}$ distorted square antiprism that is edge shared (via F1 and F3) with two $[CdF_3(H_2O)_3]^-$ octahedra (Figure 10a). The trimers connect to each other by corner-sharing via F2 atoms to create $Cd_2HfF_8(H_2O)_6$ layers (Figure 10b and 10c). In these sheets, the three water molecules and F4 atoms function as terminal ligands. The layered structure is held together by inter-layer and intra-layer hydrogen bonding between F4–H and F2–H/F3–H, respectively (Figure 10d).

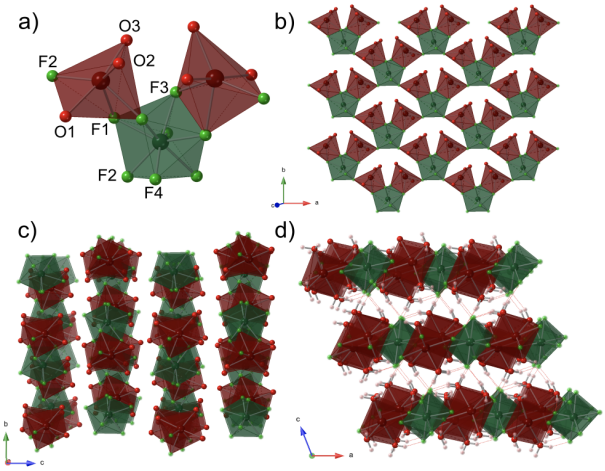


Figure 10. $[Cd_2HfF_{10}(H_2O)_6]^{2-}$ trimer (a). View of a single layer of $[Cd_2HfF_8(H_2O)_3]$ (b). View of $Cd_2HfF_8(H_2O)_3$ down the *a* axis (c). View of $Cd_2HfF_8(H_2O)_3$ down the *b* axis with hydrogen bonds shown (d). Cd, Hf, F, and O atoms are shown in maroon, dark green, light green, and red spheres, respectively. Note that H atoms in pink spheres are only shown in (d) for clarity.

*Comparison of Crystal Structures and Crystal Growth Techniques of $ABX_6$ and $A_2BX_8$ Family*

It is evident from the literature that a vast number of phases exist that have $ABX_6$ and $A_2BX_8$ stoichiometries. Furthermore, it is also apparent that subtle changes in the synthesis parameters can result in different crystal structure arrangements. In Table 2, we have tabulated the structure types, space groups, synthesis methods, and synthesis temperatures for fluoridozirconates and fluoridohafnates reported in the literature. For easier comparisons, the tabulated compounds were limited to alkaline-earth metal, lead, and cadmium containing compositions. Note that the synthesis temperature here denotes the temperature used in the reaction setup to obtain the products, not the compounds' formation temperature. In addition, compositions *7* and *13* are both named α-$SrZrF_6$ in their respective journal articles. The structures of the two compositions are, however, distinct based on the crystal system and space group. Figure 11 illustrates the synthesis temperature vs. composition index plot according to Table 2. In this plot, the numbering scheme identifying compositions (italicized) is that found in Table 2 and does not correspond to the bolded numbers used previously to identify the new compositions reported herein.

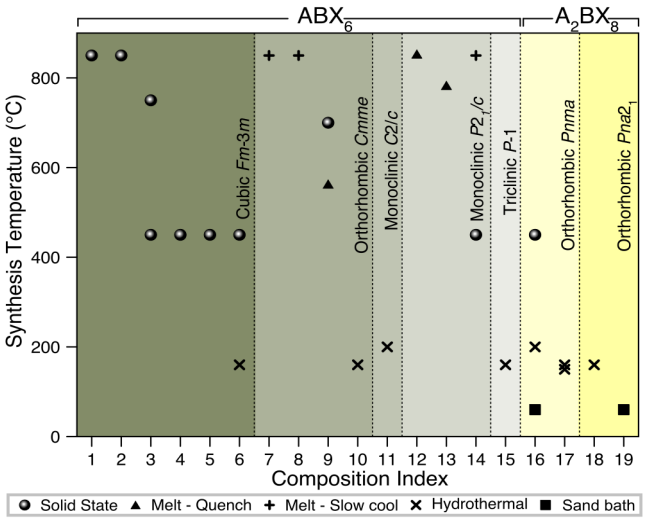


Figure 11. The synthesis temperature vs. Composition index plot. Refer to Table 2 for the composition index.

Table 2. Compounds and synthesis data in the literature and this work

| Composition Index | Composition | Structure Type | Crystal System, Space group | Method | Synthesis Temperature (°C) | Ref. No. |
|---|---|---|---|---|---|---|
| *1* | $MgZrF_6$ | $NaSbF_6$ (double-$ReO_3$) | Cubic, *Fm*–3*m* | solid state | 850 | ([47]) |
| *2* | $CaHfF_6$ | | | solid state | 850 | ([48]) |
| *3* | $CaZrF_6$ | | | solid state | 750 | ([48]) |
| | | | | | 450 | ([5]) |
| *4* | $CdZrF_6$ | | | solid state | 450 | ([5]) |
| *5* | $CdHfF_6$ | | | solid state | 450 | ([5]) |
| *6* | $MgHfF_6$ | | | solid state | 450 | ([5]) |
| | | | | hydrothermal | 160 | This work |
| *7* | α-$SrZrF_6$ | $RbPaF_6$ | Orthorhombic, *Cmme* | melt - slow cool | 850 | ([49]) |
| *8* | $PbZrF_6$ | | | melt - slow cool | 850 | ([49]) |
| *9* | β-$BaZrF_6$ | | | solid state | 700 | ([43]) |
| | | | | melt - quench | 560 | ([49]) |
| *10* | *o*-$SrHfF_6$ | | | hydrothermal | 160 | This work |
| *11* | γ-$BaZrF_6$ | *N/A* | Monoclinic, *C*2/*c* | hydrothermal | 200 | ([50]) |
| *12* | α-$SrHfF_6$ | *N/A* | Monoclinic, $P2_1/c$ | melt - quench | 850 | ([41]) |
| *13* | α-$SrZrF_6$ | | | melt - quench | 780 | ([41]) |
| *14* | α-$BaZrF_6$ | | | melt - slow cool | 850 | ([49]) |
| | | | | solid state | 450 | ([51]) |
| *15* | *t*-$SrHfF_6$ | α-$BaTbF_6$ | Triclinic, *P*–1 | hydrothermal | 160 | This work |
| *16* | α-$Ba_2ZrF_8$ | $Ba_2ZrF_8$ | Orthorhombic, *Pnma* | solid state | 450 | ([42]) |
| | | | | hydrothermal | 200 | ([42]) |
| | | | | sand bath | 60 | ([42]) |
| *17* | $Ba_2HfF_8$ | | | hydrothermal | 160 | This work |
| | | | | hydrothermal | 150 | ([8]) |
| *18* | $Pb_2HfF_8$ | *N/A* | Orthorhombic, $Pna2_1$ | hydrothermal | 160 | This work |
| *19* | $Pb_2ZrF_8$ | | | sand bath | 60 | ([42]) |

*$ABX_6$ Family*

The $ABX_6$ phases crystallize in crystal systems ranging from simple cubic to triclinic (Figure 12). These crystal systems have unique crystal structures that exhibit significant differences in their crystallographic arrangements. All compositions (*1-6* in Table 2) that take on the cubic crystal system, crystallize in the double $ReO_3$ or $NaSbF_6$ structure type (Figure 12). In this structure the Hf/Zr cations are located in an octahedral coordination environment instead of the more typical 8-coordinate arrangement expected for size of these cations. Consequently, the $A^{II}$ cation in this cubic system is limited to cations with smaller ionic radii ($Mg^{2+}$ = 0.72 Å, $Cd^{2+}$ = 0.95 Å, and $Ca^{2+}$ = 1.00 Å; Figure 13). Previously all cubic compositions were obtained via the solid-state synthesis route and now we have shown that also the mild hydrothermal approach can also be used to obtain cubic compositions, such as $MgHfF_6$.

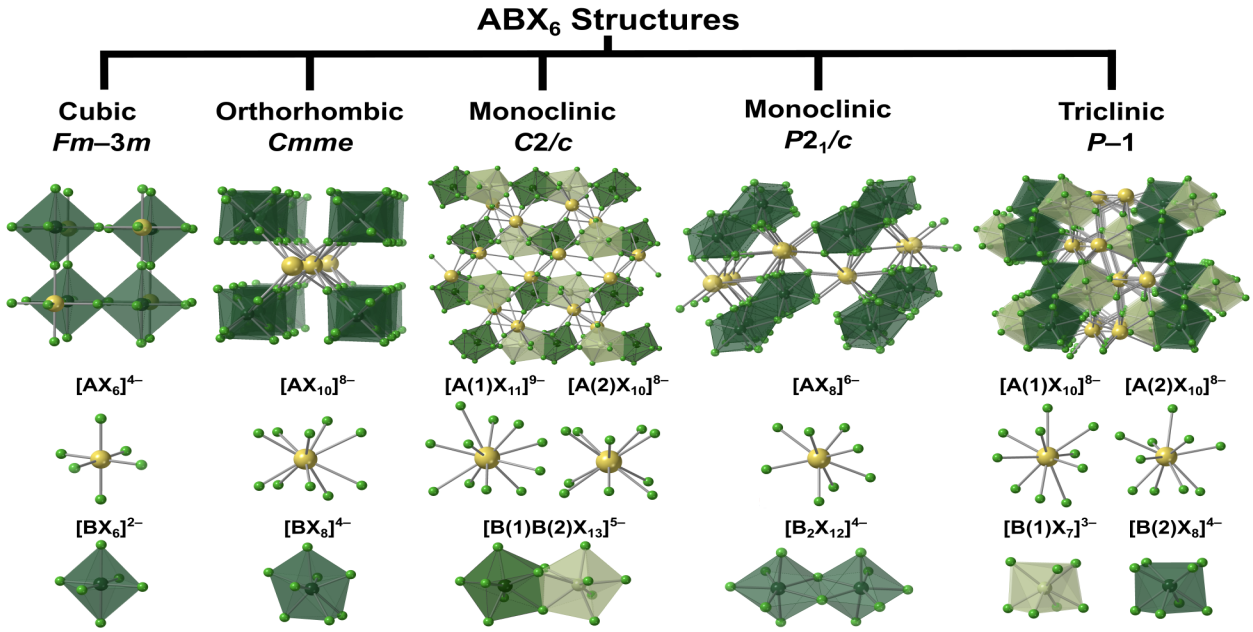


Figure 12. Comparison of the $ABX_6$ phases reported for fluoridozirconates and fluoridohafnates. The A cations are shown in yellow spheres. Note that two shades of green are used to distinguish crystallographically unique B cation sites and X anions are shown in light green spheres.

Compositions *7-15* in Table 2 contain strontium, barium, and lead and crystallize with an $ABX_6$ composition. In 1983, Kawamoto et al. synthesized several phases of $AZrF_6$ (A = Sr, Ba and Pb) using stoichiometric melts, including the low-temperature phases of α-$SrZrF_6$(*7*), $PbZrF_6$(*8*), and α-$BaZrF_6$(*14*), by melting stoichiometric ratios of starting reagents at 850 °C followed by slow

cooling. The high-temperature phases of β-$SrZrF_6$ and β-$BaZrF_6$(*9*) were obtained by crystalizing the stoichiometric melts a few degrees above their melting points followed by quenching using liquid nitrogen. However, they were unable to determine the crystal structure of β-$SrZrF_6$ and, therefore, it is not included in Table 2.[49] Surprisingly they observed that the low-temperature phases of α-$SrZrF_6$(*7*), $PbZrF_6$(*8*), and the high-temperature β-$BaZrF_6$(*9*) are isostructural and related to the $RbPaF_6$ structure (Figure 12), unlike the low-temperature α-$BaZrF_6$ (*14*), which crystallizes in the monoclinic $P2_1/c$ space group. Later studies by Laval et al. in 2018 reported the synthesis of the high-temperature phases of α-$SrHfF_6$(*12*) and α-$SrZrF_6$(*13*) that also crystallize in the monoclinic $P2_1/c$ space group. Compositions *12* and *13* were synthesized by heating stoichiometric melts to the tabulated temperatures in Table 2 and then quenching them with water. We presume that the high-temperature α-$SrZrF_6$(*12*) phase mentioned by Laval et al. is the same phase as the high-temperature β-$SrZrF_6$ reported by Kawamoto et al. The monoclinic $P2_1/c$ phase contains $[BF_7]^{3-}$ (B = Hf and Zr) pentagonal bipyramids and $[AF_8]^{6-}$ (A = Sr and Ba) snub disphenoids. Both $[AF_8]^{6-}$ and $[BF_7]^{3-}$ form edge-sharing dimers and these dimers are corner and edge shared with each other to form the three-dimensional structure. The structure is an anion excess $ReO_3$-related phase (Figure 12). An in-depth crystal structure description is given by Laval et al.[41]

In addition to the α- and β- phases of $BaZrF_6$, a third phase, γ-$BaZrF_6$(*11*), was discovered by Le Bail et al. in 1992 using hydrothermal synthesis. The phase was isolated at 200 °C, a significantly lower temperature than the α- and β- phases of $BaZrF_6$ (Figure 11). The γ-$BaZrF_6$ crystallizes in the monoclinic $C2/c$ space group and contains isolated infinite chains of $[ZrF_8]^{3-}$ distorted bicapped trigonal prisms that are linked alternatively by faces and opposite vertices (Figure 12). It is also reported that upon heating γ-$BaZrF_6$ undergoes an irreversible phase transition at 545 °C and yields α-$BaZrF_6$.[50] This is in contrast to the α-$BaZrF_6$ to β-$BaZrF_6$ phase transition at 565 °C, which is reversible.[41, 49, 50] This low-temperature γ-$BaZrF_6$ phase was only accessible via the hydrothermal route.

The final structure discussed under the $ABX_6$ family here is the *t*-$SrHfF_6$(*15*), which crystallizes in the triclinic $P\bar{1}$ space group. While we did not find any other fluoridozirconates or fluoridohafnates reported with this crystal structure, there are reports of α-$BaTbF_6$, which is isotypic (Figure 12).[52] Similar to the γ-$BaZrF_6$, *t*-$SrHfF_6$ also was only accessible via the

hydrothermal route, suggesting that both compounds are low-temperature kinetic phases (Figure 11). Beyond the crystal structure types we discussed under fluoridozirconates and fluoridohafnates, there are a plethora of materials with the $ABX_6$ formula that contain additional B cations, such as $U^{4+}$, $Th^{4+}$, $Tb^{4+}$, and $Te^{4+}$. An extensive review of other types of $ABX_6$ structures can be found in the studies by Laval et. al.[41, 53, 54]

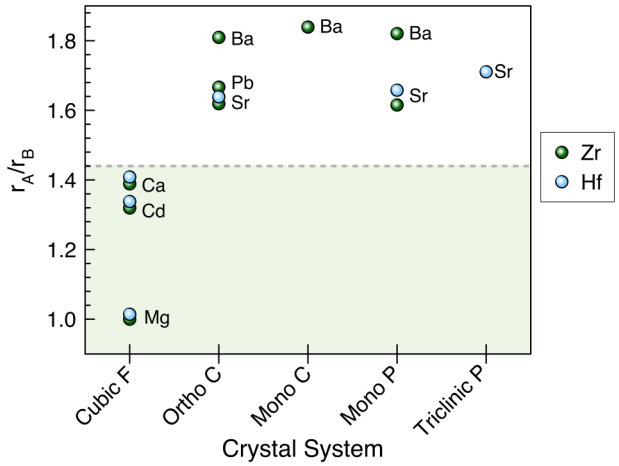


Figure 13. Radius ratio plot for $ABX_6$ phases. The $AZrF_6$ compositions are shown in green spheres while $AHfF_6$ compositions are in blue spheres.

Although we do not observe a specific trend based on the synthesis temperature vs. compositions (Figure 11) for the $ABX_6$ family, it is evident that most of these compounds are kinetic phases that are part of a large phase space. Therefore, small parameter changes in synthesis conditions result in entirely different crystal structures. However, considering the radius ratio ($r_A/r_B$) between the A and B cations for the tabulated compositions, one could observe that there is a threshold value of ~1.41 for the cubic system (Figure 13). Note that average values of Shannon ionic radii were considered for the cases in which there were multiple coordination environments for the A and B cations.[55] When $r_A/r_B$ is greater than 1.41, the phases tend to form structures in crystal systems that are lower in symmetry. This may be due to the larger A cation radii creating steric hindrance in the cubic system. More studies on fluoridozirconates and fluoridohafnates need to be carried out to arrive at a more definitive conclusion.

*$A_2BX_8$ Family*

Based on the literature, we observed that the $A_2BX_8$ compositions (*16-19* in Table 2) are only adopted by the larger $A^{II}$ cations, such as Sr, Ba, and Pb. Even though crystal structures of $Sr_2ZrF_8$ and $Sr_2HfF_8$ are not reported in the literature, there are reports by Laval et al. in 2018 of multiple microphases of $Sr_{1-x}Zr_xF_{2+2x}$ ($0.333 \leq x \leq 0.353$) that are related to the α-$Ba_2ZrF_8$ structure.[41, 56] Both α-$Ba_2ZrF_8$, $Ba_2HfF_8$, and $Sr_{1-x}Zr_xF_{2+2x}$ microphases crystallize in the orthorhombic *Pnma* space group while $Pb_2ZrF_8$ and $Pb_2HfF_8$ crystallize in the orthorhombic space group $Pna2_1$. As mentioned earlier in the text, the subtle changes in the space groups occur due to the stereochemical influence of the $6s^2$ lone pair on Pb; otherwise, these phases can be considered as belonging to the same structural series.[42, 56]

Earlier studies by Le Bail et al. in 1998 discovered α-$Ba_2ZrF_8$ and $Pb_2ZrF_8$ using multiple synthesis methods.[42] In this study, they synthesized $Ba_2ZrF_8$ via solid state (450 °C), hydrothermal (200 °C), and the direct reaction of stoichiometric ratios of $BaF_2$ and $ZrF_4$ in a sand bath (60 °C). They achieved the formation of $Pb_2ZrF_8$ only when using the sand bath method at 60 °C.[42] See Table 2. The powder samples of $Sr_{1-x}Zr_xF_{2+2x}$ microphases were synthesized via the direct reaction between $SrF_2$ and anhydrous $ZrF_4$ at 850 °C followed by slow cooling.[56] The study mentioned that prolonged annealing of these phases at temperatures lower than 400 °C led to phase decomposition; indicating that these phases are metastable. In contrast, $Ba_2HfF_8$ was reported to form only via the mild hydrothermal route by us at 160 °C and by Li et al. at 150 °C.[8] Except for the $Sr_{1-x}Zr_xF_{2+2x}$ microphases, all $A_2BX_8$ phases were synthesized in the lower temperature region of 60–450 °C. According to Figure 11, it is evident that the mild hydrothermal synthesis method is the most convenient way to obtain the majority of $A_2BX_8$ phases.

## Conclusions

Herein, we presented the synthesis and the crystal structure descriptions for seven ternary hafnium-containing fluorides. The mild hydrothermal synthetic route was employed to achieve low-temperature phase formation of fluoridohafnates. In this study, we observed that while the formulas are often isotypic, the crystal structures differ significantly. In the case of $MgHfF_6$, *o*-$SrHfF_6$, and *t*-$SrHfF_6$, the ionic radii of the alkaline-earth metal appears to impact the change from cubic $MgHfF_6$ to orthorhombic and triclinic $SrHfF_6$ phases. The occurrence of two phases of $SrHfF_6$ is likely the result of kinetic effects commonly observed in mild hydrothermal syntheses.

On the other hand, the difference in space groups in $Ba_2HfF_8$ and $Pb_2HfF_8$ is thought to be mainly due to the stereochemical influence of the $Pb^{2+}$ lone pair.

The review of existing fluoridozirconates and fluoridohafnates in literature reveals that there is no consistent relationship between different crystal systems of the $ABX_6$ family and their synthesis temperature, but rather it seems more closely connected to the cation radius ratio. For cubic compositions, a threshold radius ratio value of 1.41 is observed; greater than 1.41, the compositions crystallize in lower crystal symmetries. Many of these compositions in both the $ABX_6$ and $A_2BX_8$ families are metastable or kinetic phases. Therefore, the mild hydrothermal method is likely a better synthetic route than the solid-state synthesis method to access these low-temperature kinetic phases of fluoridozirconates and fluoridohafnates. Optimizing the mild hydrothermal method is expected to lead to the discovery of additional ternary hafnium/zirconium fluoride structures and result in an enhanced understanding of the different crystal systems present in this phase space.

## Acknowledgment

Financial support for this work was provided by the National Science Foundation under DMR-2221403 and is gratefully acknowledged.

## Supporting Information

The Supporting Information is available free of charge at ???

Single crystal structure solutions and powder X-ray diffraction patterns.

## Accession Codes

CCDC **2217961-2217967** contains the supplementary crystallographic data for this paper. These data can be obtained free of charge via www.ccdc.cam.ac.uk/data_request/cif, or by emailing data_request@ccdc.cam.ac.uk, or by contacting The Cambridge Crystallographic Data Centre, 12 Union Road, Cambridge CB2 1EZ, UK; fax: +44 1223 336033.

## References


1. Leblanc, M.; Maisonneuve, V.; Tressaud, A. Crystal Chemistry and Selected Physical Properties of Inorganic Fluorides and Oxide-Fluorides. *Chem. Rev.* **2015***, 115, 1191-1254.*
2. Gorev, M. V.; Flerov, I. N.; Tressaud, A.; Bogdanov, E. V.; Kartashev, A. V.; Bayukov, O. A.; Eremin, E. V.; Krylov, A. S. Heat Capacity and Magnetic Properties of Fluoride $CsFe^{2+}Fe^{3+}F_6$ with Defect Pyrochlore Structure. *J. Solid State Chem.* **2016***, 237, 330-335.*
3. Flerov, I. N.; Gorev, M. V.; Aleksandrov, K. S.; Tressaud, A.; Grannec, J.; Couzi, M. Phase Transitions in Elpasolites (Ordered Perovskites). *Mater. Sci. Eng. R Rep.* **1998***, 24, 81-151.*
4. Paulusz, A. G. The Predictive Use of the Configurational Co-ordinate Model for Luminescent Centres. *J. Lumin.* **1978***, 17, 375-384.*
5. Bandemehr, J.; Baumann, D.; Seibald, M.; Eklund, K.; Karttunen, A. J.; Kraus, F. Mn(IV)-Substituted Metal(II) Hexafluorido Metallates(IV): Synthesis, Crystal Structures, and Luminescence Properties. *Eur. J. Inorg. Chem.* **2021***, 2021, 3861-3869.*
6. Hall, W.; Kim, S.; Zubieta, J.; Walton, E. G.; Brown, D. B. Structure of a Mixed-Valence Iron Fluoride, $Fe_2F_5$. $2H_2O$. *Inorg. Chem.* **1977***, 16, 1884-1887.*
7. Keerthisinghe, N.; Klepov, V. V.; Zhang, E.; Smith, M. D.; Egodawatte, S.; Foulger, S. H.; zur Loye, H.-C. Hydrothermal Synthesis and Properties of $MMF_5(H_2O)_7$ ($M = Co^{2+}$ and $Ni^{2+}$, $M = Mn^{3+}$, $Ga^{3+}$, and $In^{3+}$). *Solid State Sci.* **2020***, 108, 106374.*
8. Li, H.; Yang, Z.; Luo, L.; Wang, Q.; Chen, Y.; Rong, M.; Zhou, Q.; Wang, Z. A Red-Emitting Phosphor $Ba_2HfF_8:Mn^{4+}$ with a Strengthened zero Phonon Line of $Mn^{4+}$ for Displays. *Opt. Mater.* **2020***, 107, 110091.*
9. Comer, S.; McMillen, C. D.; Kolis, J. W. Hydrothermal Growth of $LiLuF_4$ Crystals and New Lithium Lutetium Fluorides $LiKLuF_5$ and $LiNaLu_2F_8$. *Solid State Sci.* **2013***, 17, 90-96.*
10. Ketchum, D. R.; Schimek, G. L.; Pennington, W. T.; Kolis, J. W. Synthesis of New Group III Fluoride–Ammonia Adducts in Supercritical Ammonia: Structures of $AlF_3(NH_3)_2$ and $InF_2(NH_2)(NH_3)$. *Inorganica Chim. Acta.* **1999***, 294, 200-206.*
11. McMillen, C. D.; Kolis, J. W. Bulk Single Crystal Growth from Hydrothermal Solutions. *Philosophical Magazine.* **2012***, 92, 2686-2711.*
12. Cansell, F.; Chevalier, B.; Demourgues, A.; Etourneau, J.; Even, C.; Pessey, V.; Petit, S.; Tressaud, A.; Weill, F. Supercritical Fluid Processing: A New Route for Materials Synthesis. *J. Mater. Chem.* **1999***, 9, 67-75.*
13. Bugaris, D. E.; zur Loye, H.-C. Materials Discovery by Flux Crystal Growth: Quaternary and Higher Order Oxides. *Angew. Chem. Int. Ed.* **2012***, 51, 3780-3811.*
14. Klepov, V. V.; Juillerat, C. A.; Pace, K. A.; Morrison, G.; zur Loye, H.-C. "Soft" Alkali Bromide and Iodide Fluxes for Crystal Growth. *Front Chem.* **2020***, 8, 518.*
15. Latshaw, A. M.; Wilkins, B. O.; Morrison, G.; Smith, M. D.; zur Loye, H.-C. $A_5RE_4X[TO_4]_4$ Crystal Growth: Fluoride Flux Synthesis of $Na_5Ln_4F[GeO_4]_4$ (Ln=Pr, Nd), the First Quaternary Germanate Oxyfluorides. *J. Solid State Chem.* **2016***, 239, 200-203.*
16. Spagnuolo, N. R.; Morrison, G.; zur Loye, H.-C. Synthesis and Crystal Structure of $[(Cs_6F)(Cs_3AgF)][Ge_{14}O_{32}]$ Through Alkali Halide Flux Growth. *Solid State Sci.* **2019***, 97, 105973.*
17. Latshaw, A. M.; Wilkins, B. O.; Hughey, K. D.; Yeon, J.; Williams, D. E.; Tran, T. T.; Halasyamani, P. S.; zur Loye, H.-C. $A_5RE_4X[TO_4]_4$ Crystal Growth and

Photoluminescence. Fluoride Flux Synthesis of Sodium and Potassium Rare Earth Silicate Oxyfluorides. *CrystEngComm.* **2015***, 17, 4654-4661.*
18. Juillerat, C. A.; Klepov, V. V.; Morrison, G.; Pace, K. A.; zur Loye, H.-C. Flux Crystal Growth: A Versatile Technique to Reveal the Crystal Chemistry of Complex Uranium Oxides. *Dalton Trans.* **2019***, 48, 3162-3181.*
19. Carone, D.; Klepov, V. V.; Misture, S. T.; Schaeperkoetter, J. C.; Jacobsohn, L. G.; Aziziha, M.; Schorne-Pinto, J.; Thomson, S. A. J.; Hines, A. T.; Besmann, T. M.; zur Loye, H.-C. Luminescence and Scintillation in the Niobium Doped Oxyfluoride $Rb_4Ge_5O_9F_6$:Nb. *Inorganics.* **2022***, 10, 83.*
20. Klepov, V. V.; Felder, J. B.; zur Loye, H.-C. Synthetic Strategies for the Synthesis of Ternary Uranium(IV) and Thorium(IV) Fluorides. *Inorg. Chem.* **2018***, 57, 5597-5606.*
21. Carone, D.; Morrison, G.; Smith, M. D.; zur Loye, H.-C. Crystal Growth of New Germanate Framework Structures: Impact of the Presence of Square Planar Copper Species and Mixed Ge/Mn Sites on the Overall Structures of $Rb_2Cu_3Ge_5O_{14}$, $Cs_2Cu_3Ge_5O_{14}$, $Cs_7Cu_2Ge_{11}O_{27}F$, and $[(Cs_6F)(Cs_3AgF)][Ge_{12}Mn_2O_{32}]$. *Cryst. Growth Des.* **2022***, 22, 3319-3325.*
22. Carone, D.; Usman, M.; Klepov, V. V.; Smith, M. D.; Kocevski, V.; Besmann, T. M.; zur Loye, H.-C. New Germanate and Mixed Cobalt Germanate Salt Inclusion Materials: $[(Rb_6F)(Rb_4F)][Ge_{14}O_{32}]$ and $[(Rb_6F)(Rb_{3.1}Co_{0.9}F_{0.96})][Co_{3.8}Ge_{10.2}O_{30}F_2]$. *CrystEngComm.* **2020***, 22, 8072-8080.*
23. Keerthisinghe, N.; Berseneva, A. A.; Klepov, V. V.; Morrison, G.; zur Loye, H.-C. A Geometrically Frustrated Family of $M^{II}M^{III}F_5(H_2O)_2$ Mixed-Metal Fluorides with Complex Magnetic Interactions. *Inorg. Chem.* **2021***, 60, 14318-14329.*
24. Yeon, J.; Smith, M. D.; Tapp, J.; Möller, A.; zur Loye, H.-C. Application of a Mild Hydrothermal Approach Containing an in situ Reduction Step to the Growth of Single Crystals of the Quaternary U(IV)-Containing Fluorides $Na_4MU_6F_{30}$ ($M = Mn^{2+}$, $Co^{2+}$, $Ni^{2+}$, $Cu^{2+}$, and $Zn^{2+}$) Crystal Growth, Structures, and Magnetic Properties. *J. Am. Chem. Soc.* **2014***, 136, 3955-3963.*
25. Ayer, G. B.; Klepov, V. V.; Smith, M. D.; Hu, M.; Yang, Z.; Martin, C. R.; Morrison, G.; zur Loye, H.-C. $BaWO_2F_4$: A Mixed Anion X-Ray Scintillator with Excellent Photoluminescence Quantum Efficiency. *Dalton Trans.* **2020***, 49, 10734-10739.*
26. Yeon, J.; Smith, M. D.; Tapp, J.; Möller, A.; zur Loye, H.-C. Mild Hydrothermal Crystal Growth, Structure, and Magnetic Properties of Ternary U(IV) Containing Fluorides: $LiUF_5$, $KU_2F_9$, $K_7U_6F_{31}$, $RbUF_5$, $RbU_2F_9$, and $RbU_3F_{13}$. *Inorg. Chem.* **2014***, 53, 6289-6298.*
27. Pace, K. A.; Klepov, V. V.; Morrison, G.; zur Loye, H.-C. Moderate Supercritical Synthesis as a Facile Route to Mixed-Valent Uranium(IV, V) and (V, VI) Silicates. *Chem Commun (Camb).* **2018***, 54, 13794-13797.*
28. Yeon, J.; Smith, M. D.; Morrison, G.; zur Loye, H.-C. Trivalent Cation-Controlled Phase Space of New U(IV) Fluorides, $Na_3MU_6F_{30}$ ($M = Al^{3+}$, $Ga^{3+}$, $Ti^{3+}$, $V^{3+}$, $Cr^{3+}$, $Fe^{3+}$): Mild Hydrothermal Synthesis Including an in situ Reduction Step, Structures, Optical, and Magnetic properties. *Inorg. Chem.* **2015***, 54, 2058-2066.*
29. Klepov, V. V.; Pace, K. A.; Berseneva, A. A.; Felder, J. B.; Calder, S.; Morrison, G.; Zhang, Q.; Kirkham, M. J.; Parker, D. S.; zur Loye, H.-C. Chloride Reduction of $Mn^{3+}$ in Mild Hydrothermal Synthesis of a Charge Ordered Defect Pyrochlore, $CsMn^{2+}Mn^{3+}F_6$, a Canted Antiferromagnet with a Hard Ferromagnetic Component. *J. Am. Chem. Soc.* **2021***, 143, 11554-11567.*

30. Deason, T. K.; Morrison, G.; Mofrad, A.; Tisdale, H. B.; Amoroso, J.; DiPrete, D.; Was, G.; Sun, K.; Besmann, T. M.; zur Loye, H.-C. Developing Waste Forms for Transuranic Elements: Quaternary Neptunium Fluorides of the Type $NaMNp_6F_{30}$ (M = Ti, V, Cr, Mn, Fe, Co, Ni, Al, Ga). *J. Am. Chem. Soc.* **2023***, 145, 465-475.*
31. Pace, K. A.; Klepov, V. V.; Deason, T. K.; Smith, M. D.; Ayer, G. B.; Diprete, D. P.; Amoroso, J. W.; zur Loye, H.-C. Expansion of the $Na_3M^{III}(Ln/An)_6F_{30}$ Series: Incorporation of Plutonium into a Highly Robust and Stable Framework. *Chemistry.* **2020***, 26, 12941-12944.*
32. Ayer, G. B.; Morrison, G.; Smith, M. D.; Jacobsohn, L. G.; zur Loye, H.-C. Luminescence and Scintillation of $[Nb_2O_2F_9]^{3-}$-Dimer-Containing Oxide-Fluorides: $Cs_{10}(Nb_2O_2F_9)_3F$, $Cs_{9.4}K_{0.6}(Nb_2O_2F_9)_3F$, and $Cs_{10}(Nb_2O_2F_9)_3Cl$. *Inorg. Chem.* **2022***, 61, 3256-3262.*
33. Ayer, G. B.; Klepov, V. V.; Pace, K. A.; zur Loye, H.-C. Quaternary Cerium(iv) Containing Fluorides Exhibiting $Ce_3F_{16}$ Sheets and $Ce_6F_{30}$ Frameworks. *Dalton Trans.* **2020***, 49, 5898-5905.*
34. Ayer, G. B.; Klepov, V. V.; Smith, M. D.; zur Loye, H.-C. Mild Hydrothermal Synthesis of the Complex Hafnium-Containing Fluorides $Cs_2[M(H_2O)_6][Hf_2F_{12}]$ (M = Ni, Co, Zn), $CuHfF_6(H_2O)_4$, and $Cs_2Hf_3Mn_3F_{20}$ Based on $HfF_7$ and $HfF_6$ Coordination Polyhedra. *Inorg. Chem.* **2019***, 58, 13049-13057.*
35. APEX3 Version 2019.1-0 and SAINT+ Version 8.40A. **2019**.
36. Krause, L.; Herbst-Irmer, R.; Sheldrick, G. M.; Stalke, D. Comparison of Silver and Molybdenum Microfocus X-ray Sources for Single-Crystal Structure Determination. *J. Appl. Crystallogr.* **2015***, 48, 3-10.*
37. Dolomanov, O. V.; Bourhis, L. J.; Gildea, R. J.; Howard, J. A. K.; Puschmann, H. OLEX2: A Complete Structure Solution, Refinement and Analysis Program. *J. Appl. Crystallogr.* **2009***, 42, 339-341.*
38. Sheldrick, G. M. SHELXT– Integrated Space-Group and Crystal-Structure Determination. *Acta Cryst. A.* **2015***, 71, 3-8.*
39. Hübschle, C. B.; Sheldrick, G. M.; Dittrich, B. ShelXle: A Qt Graphical User Interface for SHELXL. *J. Appl. Crystallogr.* **2011***, 44, 1281-1284.*
40. Kraus, M.; Müller, M.; Fischer, R.; Schmidt, R.; Koller, D.; Müller, B. G. Single Crystal Synthesis and Structure of Various Transition Metal Fluorides with Divalent and Tetravalent Cations. *J. Fluor. Chem.* **1999***, 165-171.*
41. Laval, J.-P.; Mayet, R. High-Temperature Monoclinic α-$SrHfF_6$, and Isostructural α-$SrZrF_6$: Associating $Hf_2F_{12}$ Bipolyhedra and $SrF_8$ Snub Disphenoids. *Acta Cryst. C.* **2018***, 74, 229-235.*
42. Le Bail, A.; Laval, J.-P. Synthesis and Crystal Structure of α-$Ba_2ZrF_8$ and $Pb_2ZrF_8$ Determined ab initio from Synchrotron and Neutron Powder Diffraction Data. *Eur. J. Solid State Inorg. Chem.* **1998***, 35, 357-372.*
43. Mehlhorn, B.; Hoppe, R. New Hexafluorozirconates(IV): $BaZrF_6$, $PbZrF_6$, $EuZrF_6$, $SrZrF_6$. *Z. Anorg. Allg. Chem.* **1976***, 425, 180-188.*
44. Xu, J.; Hu, L.; Song, Y.; Han, F.; Qiao, Y.; Deng, J.; Chen, J.; Xing, X. Zero Thermal Expansion in Cubic $MgZrF_6$. *J. Am. Ceram. Soc.* **2017***, 100, 5385-5388.*
45. Oudahmane, A.; El-Ghozzi, M.; Avignant, D. $Ca_5Zr_3F_{22}$. *Acta Crystallogr. Sect. E.* **2012***, 68, 23.*
46. Le Bail, A. Structure of $Sr_5Zr_3F_{22}$ Determined from an Inversion Twinned Crystal. *Eur. J. Solid State Inorg. Chem.* **1996***, 33, 1211-1222.*

47. Gerasimenko, A. V.; Gaivoronskaya, K. A.; Slobodyuk, A. B.; Didenko, N. A. Magnesium Hexafluoidozirconates $MgZrF_6.5H_2O$, $MgZrF_6.2H_2O$ and $MgZrF_6$: Structures, Phase Transitions, and Internal Mobility of Water Molecules. *Z. Anorg. Allg. Chem.* **2017***, 643, 1785-1792.*
48. Hancock, J. C.; Chapman, K. W.; Halder, G. J.; Morelock, C. R.; Kaplan, B. S.; Gallington, L. C.; Bongiorno, A.; Han, C.; Zhou, S.; Wilkinson, A. P. Large Negative Thermal Expansion and Anomalous Behavior on Compression in Cubic $ReO_3$-Type $A^{II}B^{IV}F_6$: $CaZrF_6$ and $CaHfF_6$. *Chem. Mater.* **2015***, 27, 3912-3918.*
49. Kawamoto, Y.; Sakaguchi, F. Thermal Properties and Raman Spectra of Crystalline and Vitreous $BaZrF_6$, $PbZrF_6$ and $SrZrF_6$. *Bull. Chem. Soc. Jpn.* **1983***, 56, 2138-2141.*
50. Le Bail, A.; Mercier, A. M. Synthesis and Crystal Structure of γ-$BaZrF_6$. *J. Solid State Chem.* **1992***, 101, 229-236.*
51. Laval, J.-P.; Papiernik, R.; Frit, B. $BaZrF_6$α: A Complex Anion Structure $[Zr_2F_{12}]^{4-}$. *Acta Cryst. B.* **1978***, 34, 1070-1074.*
52. Largeau, E.; Gaumet, V.; El-Ghozzi, M.; Avignant, D.; Cousseins, J. C. Synthesis and Single-Crystal Structural Study of an Original Low-Temperature Form α of $BaTbF_6$. *J. Mater. Chem.* **1997***, 7, 1881-1885.*
53. Laval, J.-P.; Mayet, R.; Mikou, A. Cationic Ordering in Tysonite Type Structures: II: Crystal Structure of α-, β- and γ-Barium Hexafluoridouranates (IV). *J. Fluor. Chem.* **2017***, 193, 126-135.*
54. Ider, A.; El Farissi, M.; Laval, J.-P. Cationic Ordering in Tysonite Type Structures I: Crystal Structure of $BaTeF_6$. *J. Fluor. Chem.* **1999***, 99, 161-166.*
55. Shannon, R. D. Revised Effective Ionic Radii and Systematic Studies of Interatomic Distances in Halides and Chalcogenides. *Acta Cryst. A.* **1976***, 32, 751-767.*
56. Laval, J.-P.; Rafik, H.; Trolliard, G. Microphases Deriving from $Ba_2ZrF_8$ Structure Type: II: Crystal Structure of $Sr_{17}Zr_9F_{70}$ and $Sr_{17.145}Zr_9F_{70.29}$. *J. Solid State Chem.* **2018***, 260, 151-158.*

For Table of Contents Use Only

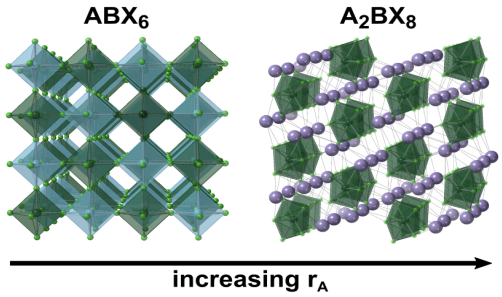


**Synopsis**

Using mild hydrothermal synthesis, a group of ternary hafnium fluorides was synthesized, and their crystal structures are compared and described. Additionally, we provide a summary of the synthesis conditions and crystal structures of previously reported fluoridohafnates and fluoridozirconates.